Visualizing Atomistic Formation Process of SrO_x Thin Films on $SrTiO_3$

Takeo Ohsawa,[†,‡,*] Ryota Shimizu,[†] Katsuya Iwaya,[†,∥] and Taro Hitosugi[†,§,*]

[†]Advanced Institute for Materials Research, Tohoku University, Sendai 980-8577, Japan, [‡]National Institute for Materials Science, 1-1 Namiki, Tsukuba 305-0044, Japan, and [§]PRESTO, Japan Science and Technology Agency, Tokyo 102-0076, Japan. [∥]Present address: RIKEN Center for Emergent Matter Science, Wako, Saitama 351-0198, Japan.

ABSTRACT Metallic conductivity observed in the heterostructure of $LaAlO_3/SrTiO_3$ has attracted great attention, triggering a debate over whether the origin is an intrinsic electronic effect or a defect-related phenomenon. One of the issues to be solved is the role of SrO layer, which turns the conductive interface into an insulator when inserted between $LaAlO_3$ and $SrTiO_3$. To understand the origins of this oxide interface phenomenon and to further explore unconventional functionalities, it is necessary to elucidate how SrO layers are formed during the initial growth process at the atomic level. Here, we atomically resolve growth processes of heteroepitaxial SrO_x films on $SrTiO_3(001)$-$(\sqrt{13} \times \sqrt{13})$-$R33.7°$ substrate using scanning tunneling microscopy/spectroscopy. On the sub-unit-cell SrO_x film surface, no periodic structure was observed as a result of random Ti incorporation into the SrO_x islands, indicating the importance of the control of excess Ti atoms on the substrate prior to deposition. This random arrangement of Ti atoms is a marked contrast to the homoepitaxy on $SrTiO_3(001)$-$(\sqrt{13} \times \sqrt{13})$-$R33.7°$. Furthermore, the formation of SrO_x islands introduced defects in the surrounding $SrTiO_3$ substrate surface. Such atom-by-atom engineering and characterizations of oxide heterostructures not only provide microscopic understanding of formation process of interfaces in metal—oxides, but also would lead to the creation of exotic electronic phenomena and novel functionalities at these interfaces.

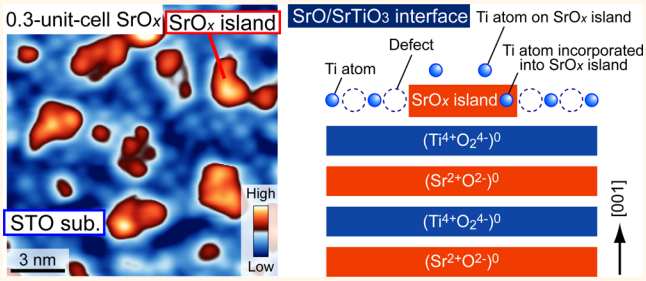

KEYWORDS: oxide thin films and interfaces · epitaxial film · surface reconstruction · initial growth process · strontium titanate · scanning tunneling microscopy · pulsed laser deposition

A striking result found in the field of metal—oxides research is the two-dimensional (2D) conductivity found at the interface between two band insulators, $LaAlO_3$ (LAO) and $SrTiO_3$ (STO).[1,2] However, the mechanism of the charge-generation at this interface is currently unclear; both the existence of critical thickness[3] and the suppression of conductivity when using SrO-terminated substrate remain two essential issues that need to be resolved to elucidate the origin of 2D conductivity. For the latter, in general, SrO-terminated surface is prepared by depositing SrO layer on a STO surface with steps and terraces. Due to the high chemical reactivity of the SrO, there has been no detailed report on this surface at the atomic level, leaving out the investigation of the role of SrO-terminated surface in LAO/STO system.

The most straightforward approach to study this surface is to directly observe the surface using scanning tunneling microscopy/spectroscopy (STM/STS). Low-temperature STM combined with pulsed laser deposition (PLD) in an ultrahigh vacuum provides us with an ideal tool for observing such situations.[4] The STM system enables us to access the surface of films without exposing their surfaces to air, and thus, intrinsic nature of SrO layer can be elucidated by the precise atomic-scale electronic structure measurement using spectroscopic imaging. To visualize the initial formation process of oxides and their interfaces, we also need to prepare an atomically defined substrate surface that is stable under thin-film growth conditions, since the widely used standard step-and-terrace STO(001) substrate[5] has disordered atomic arrangement at the surface.[6] We suggest the use of $(\sqrt{13} \times \sqrt{13})$-$R33.7°$ reconstructed STO(001) substrate as a platform of the growth studies from the following reasons: (1) structural robustness over a wide range of oxygen pressures[7] and annealing temperatures,[8,9] (2) a well-known atomic arrangement,[10] and (3) reproducibility for preparing the

* Address correspondence to ohsawa.takeo@nims.go.jp, hitosugi@wpi-aimr.tohoku.ac.jp.

Received for review October 14, 2013 and accepted February 23, 2014.

Published online February 23, 2014
10.1021/nn405359u

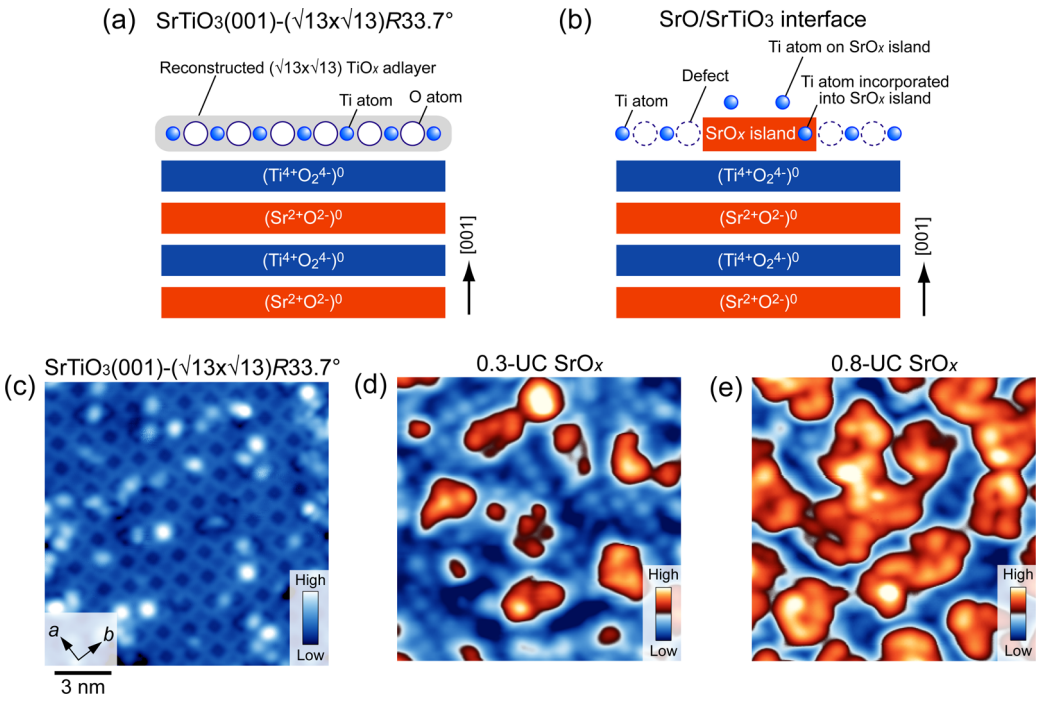

Figure 1. (a) A schematic illustration of STO(001)-($\sqrt{13} \times \sqrt{13}$)-*R*33.7° substrate studied in this study. The surface has excess Ti and O atoms that arrange in ($\sqrt{13} \times \sqrt{13}$) periodicity. (b) A schematic illustration of the SrO_x-deposited STO(001)-($\sqrt{13} \times \sqrt{13}$)-*R*33.7° surface. The formation of SrO_x islands induce defects on the surrounding substrate surface and intermix with excess Ti ions, which are distributed on the top of the SrO_x island or incorporated into the SrO_x island. (c) STM image of STO(001)-($\sqrt{13} \times \sqrt{13}$)-*R*33.7° substrate surface (V_s = +1.9 V, I_t = 30 pA, 15 × 15 nm^2), prior to the deposition of SrO_x films. (d) STM image of 0.3-UC SrO_x deposited surface (V_s = +1.9 V, I_t = 30 pA, 15 × 15 nm^2). Blue and orange areas correspond to substrate and islands, respectively. (e) STM image of 0.8-UC SrO_x deposited surface (V_s = +1.9 V, I_t = 30 pA, 15 × 15 nm^2).

reconstruction. The insights gained from the observation of ($\sqrt{13} \times \sqrt{13}$) reconstruction would represent general growth picture of oxides because other reconstructions and step-and-terrace surfaces of $SrTiO_3$ (001) also have excess Ti and O atoms on the bulk-cut TiO_2 layer. In fact, a homoepitaxial STO growth on this surface was previously demonstrated, and the identical ($\sqrt{13} \times \sqrt{13}$) structure was successfully observed on the STO film surfaces.[8]

In this article, we examine the SrO-terminated surface formed on atomically defined ($\sqrt{13} \times \sqrt{13}$)-*R*33.7° reconstructed STO(001) substrate surfaces (hereafter called RT13-STO), aiming to provide atomistic pictures of the structures and growths in comparison with those of STO homoepitaxy. These studies provide the microscopic view of the very first step to form the SrO/STO interfaces. Figure 1a,b summarizes our experimental strategy. We deposit sub-unit-cell (UC) SrO_x films on RT13-STO(001) single-crystal surface [TiO_x ($\sqrt{13} \times \sqrt{13}$ structure is formed on the top of TiO_2-terminated STO substrate,[8,10,11] Figure 1a]. On this surface, we conducted STM/STS studies, unveiling random arrangement of Ti (blue circles in Figure 1b) on SrO_x island surfaces in striking contrast to the periodic array of Ti atoms on the STO homoepitaxy case.[8] These properties are compared with the *c*(6 × 2) SrO surface[12] found on RT13-STO(001) substrate surface.[13] Furthermore, we report a surface symmetry change during the initial stage of the SrO_x film growth, due to the formation of defects. We stress that excess surface atoms on the substrate should be taken into account for the growth process of perovskite thin films. Our findings suggest that microscopic nature of thin film and interface formation process needs to be considered to account for the interface-dependent transport properties in LAO/STO heterostructures.

RESULTS AND DISCUSSION

We prepared 0.3-UC (Figure 1d) and 0.8-UC (Figure 1e) SrO_x films on the RT13-STO substrate surfaces (Figure 1c). On the deposition of 0.3-UC SrO_x, SrO_x islands distributed uniformly over the STO surface, with an average size of ~2 nm and a height of ~0.2 nm (sample bias voltage, V_s, of +1.9 V) corresponding to a half UC of the STO crystal. Although we followed the well-established procedure of typical "SrO" depositions,[14] the island is not necessarily the stoichiometric SrO due to the various and unknown chemical reaction processes expected on the target and oxide surface. We thus use the term "SrO_x islands" through this paper. These islands were smaller and anisotropic in shape than the islands observed in the homoepitaxial STO islands on RT13-STO substrate.[8] Furthermore, we notice two differences, representing the unique growth modes in the SrO_x films when compared with those of the STO homoepitaxy.[8] One is that the STO substrate

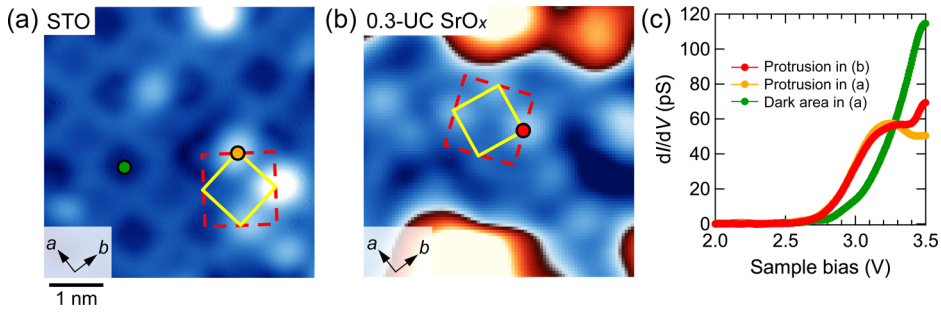

Figure 2. (a) STM image of STO substrate (V_s = +1.9 V, I_t = 30 pA, 5 × 5 nm^2). The ($\sqrt{13} \times \sqrt{13}$) structure and $c(\sqrt{13} \times \sqrt{13})$ structure are shown as a red broken line and yellow square, respectively. (b) STM image of 0.3-UC SrO_x film, focusing on surrounding STO substrate surface (V_s = +1.9 V, I_t = 30 pA, 5 × 5 nm^2). The bright protrusions are located at the atomic sites of the $c(\sqrt{13} \times \sqrt{13})$ structure, as indicated by the yellow square. The red square indicates the ($\sqrt{13} \times \sqrt{13}$) structure. (c) Differential conductance (dI/dV) spectra taken at bright protrusions in 0.3-UC SrO_x film (red) and STO substrate (orange). For comparison, the dI/dV spectrum taken at a location far from the bright protrusions in the STO substrate surface is shown (green). The bright protrusions observed in both samples exhibit a characteristic peak at around V_s = +3.2 V.

TABLE 1. Annealing Condition Dependence of the Densities of Protrusions Observed on undoped STO(001)-($\sqrt{13}\times\sqrt{13}$)-*R*33.7° Substrate Surface

condition	density of bright spots (cm^{-2})	coverage per $c(\sqrt{13}\times\sqrt{13})$
Annealed at 850 °C in UHV	5.6 × 10^{13}	0.56 ± 0.02
Annealed at 850 °C in $P(O_2)$ = 1 × 10^{-8} Torr	4.9 × 10^{13}	0.49 ± 0.02
Annealed at 850 °C in $P(O_2)$ = 1 × 10^{-6} Torr	3.4 × 10^{13}	0.34 ± 0.01

surface around the SrO_x islands was remarkably changed by the SrO_x deposition, due to the formation of defects. The other is that no periodic structure was observed on the surface of SrO_x islands, indicating that excess Ti atoms are distributed on the top of the SrO islands or are incorporated into the SrO island. These growth behaviors, which are elaborately discussed later, are a sharp contrast with those of STO homoepitaxy on RT13-STO substrate, in which layered structure of STO and TiO_x adlayer with RT13 structure was apparently evident.[8]

The former is clearly recognized when we compare the surface structure of the STO substrate before and after SrO_x film deposition. The RT13-STO substrate surface prior to the deposition shows periodic dark and faint dark squares, apparently indicating an ordered arrangement of atoms at the surface (Figure 2a, V_s = +1.9 V). On the basis of the experimental and theoretical results, this surface structure is composed of an additional TiO_x adlayer formed on a bulk-like termination of a TiO_2 plane.[10] In the close-up STM image of 0.3-UC SrO_x film obtained at V_s = +1.9 V (Figure 2b), the mesh structure observed on the RT13-STO substrate (Figure 2a) disappeared, and instead, many protrusions arranged periodically with $c(\sqrt{13} \times \sqrt{13})$ symmetry were observed. The density of the protrusions was ∼1.0 × 10^{14} cm^{-2}, which is much larger than the density of protrusions found in the RT13-STO (∼1.4 × 10^{13} cm^{-2}: Figure 2a) substrate surface prepared under the same oxygen pressure, indicating that the substrate surface atomic structure was modified by the deposition of SrO_x. Both of these protrusions have characteristic peak structure at V_s around +3.2 V in the tunneling conductance (dI/dV) spectra (Figure 2c). Furthermore, those protrusions appear in the same site on RT13-STO substrate surface, strongly suggesting that the origin is identical. We confirmed that the density of the protrusions on RT13-STO substrate monotonically increased with decreasing oxygen partial pressure, $P(O_2)$, during annealing (Table 1). Thus, a possible explanation for the protrusions is oxygen vacancies. These results may indicate that, contrasting to our intuitive sense that the substrate surface itself should be intact during or after the film deposition, Sr atoms, migrating on the surface upon initial growth of SrO_x, extract the surface oxygen in the topmost TiO_x adlayer to form SrO_x islands. This is reasonable by considering that Sr has higher affinity to oxygen than Ti in the Ellingham diagram.[15] However, any in-gap states as expected as donor states, originating from oxygen vacancies, below the conduction band were not detected. Another possible defects are, for instance, adsorbed hydrogen or hydroxyl (−OH), as observed on rutile TiO_2(110) surfaces.[16] Further investigations are necessary to identify these defects.

On the SrO_x islands of 0.3-UC and 0.8-UC films, no atomic lattice was observed (Figure 1d,e). We note that this is in sharp contrast with the homoepitaxial STO islands, where clear RT13 structure was found on the island.[8] We propose, as shown in Figure 1b, the SrO_x islands are grown directly on the bulk-cut TiO_2 layer rather than on the TiO_x adlayer of the RT13 structure. In case of the homoepitaxial STO and heteroepitaxial LAO films grown on the RT13 structure, we observed the identical RT13 structure even on the films.[8,17] These

results can be understood in terms of the transfer of the TiO_x-based RT13 structure to the top of the films, indicating the existence of abrupt SrO/TiO_2 and LaO/TiO_2 interfaces. We thus believe this growth mechanism can be also applied for SrO_x films. A possible explanation for the absence of periodic structure on SrO_x islands is that excess Ti atoms in additional TiO_x adlayer on the substrate are either located on the top of the SrO_x islands or incorporated randomly into the SrO_x islands. In fact, we observed a clear V_s dependence of height within SrO_x islands in STM images, which was not seen in the homoepitaxial STO islands. Panels a and b of Figure 3 compare STM images obtained at the same location of the 0.3-UC SrO_x film, imaged at V_s = +1.9 and +3.5 V, respectively. It is clearly seen that several sites of the SrO_x islands observed at V_s = +1.9 V diminish at +3.5 V, representing that the composition of the SrO_x islands is not uniform. This is obvious in the cross section (Figure 3c) for one of the islands in Figure 3a,b.

To understand such strong and local V_s dependence, we performed STM observations on RT13-STO single crystal substrate surface, in which both TiO_x-based RT13 structure and SrO plane [$c(6 \times 2)$] are visible,[13] as shown in panels d and e of Figure 3 imaged at V_s = +1.8 and +3.6 V, respectively. The relative height of the SrO plane compared to the TiO_x plane strongly depends on V_s, decreasing with increasing V_s (Figure 3f), and finally, the height of the SrO plane becomes identical to the level of TiO_x plane. This tendency is quite similar to that of the V_s-dependent area in the SrO_x islands; V_s-dependent relative height (ΔH) of SrO_x islands in 0.3-UC SrO_x film and SrO plane in STO substrate shows very similar bias dependence from V_s = +1.4 to +3.6 V (Figure 3g), indicating that the SrO_x islands and the SrO plane have similar compositions. Thus, strongly V_s-dependent area in the SrO_x island, for instance marked with cross in Figure 3a,b, consists of SrO, and consequently, the less-bias dependent area suggests the existence of Ti atoms in the islands. By comparing STM images at V_s = +1.9 and +3.5 V, panels a and b of Figure 3, respectively, we estimated the area composed of the excess Ti atoms in the SrO_x islands to be approximately 23% of the whole area of SrO_x islands, which is much smaller than that expected from the model in Figure.1b. This is possibly because Ti atoms hybridize with surrounding O atoms and also form clusters in the SrO_x islands, and thus, electronic structure is largely modified. We also note that this V_s dependence of SrO- and TiO_2-terminated STO (or SrO and excess Ti area in SrO_x islands) cannot be simply understood in terms of partial density of states of Sr and Ti in this energy range, since if the density of states of Sr become dominant at higher V_s, opposite V_s dependence would be expected.

To strengthen this discussion and to explain the V_s dependence of STM images, we performed local barrier height (LBH) measurements, as is applied for

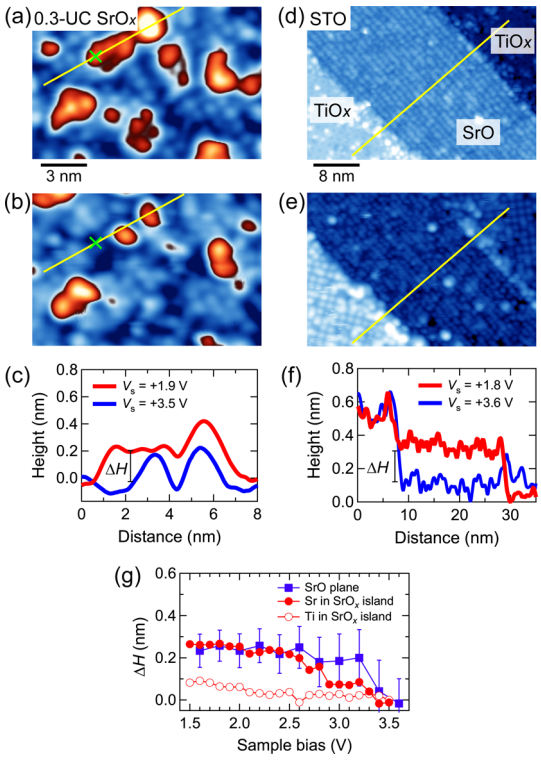

Figure 3. (a and b) Bias-dependent STM images of 0.3-UC SrO_x islands at V_s = +1.9 and +3.5 V, respectively (I_t = 30 pA, 15 × 10 nm^2). Both images were taken at the same location. (c) Line profiles across the SrO_x islands in (a) and (b). A part of the SrO_x island (marked with a cross) shows strong bias dependence, indicating that the composition of the island is not uniform. (d and e) Bias-dependent STM images of the STO substrate at V_s = +1.8 and +3.6 V (I_t = 30 pA, 40 × 27 nm^2), respectively. Both the TiO_x plane [($\sqrt{13} \times \sqrt{13}$) structure] and SrO plane [$c(6 \times 2)$] were imaged. (f) Line profiles across the SrO plane in (d) and (e). The height difference between the TiO_x and the SrO plane strongly depends on V_s. (g) Relative height (ΔH) of SrO_x islands in 0.3-UC SrO_x film and relative height of SrO_x plane in STO substrate as a function of V_s. The heights of the SrO_x islands and the SrO plane showed a similar bias dependence, indicating that the SrO_x islands and the SrO plane have similar compositions.

conventional semiconductor surfaces and metal surfaces.[18,19] In the microscopic quantum mechanical regime, namely, in the atomic-resolution STM measurements, it is known that the LBHs can be attributed to decay rates of the surface wave functions, rather than local work functions at the surface.[20] The decay rates (or LBHs) are determined mainly by local chemical properties at the surface. For the STO substrate, the TiO_x adlayer [RT13 structure] and the SrO layer [$c(6 \times 2)$] are clearly distinguishable in the LBH image (Figure 4a) because the LBHs of those layers exhibit not only different values but also different V_s dependences (Figure 4b). The LBH of the SrO layer was higher than that of the TiO_x adlayer at V_s ranging from +1.6 to +3.6 V. In addition, both the LBH values gradually decreased with increasing V_s, which is a typical behavior due to the biasing effect of the tunneling barrier as observed in conventional semiconductor surfaces,[20] and the LBH difference between the two layers

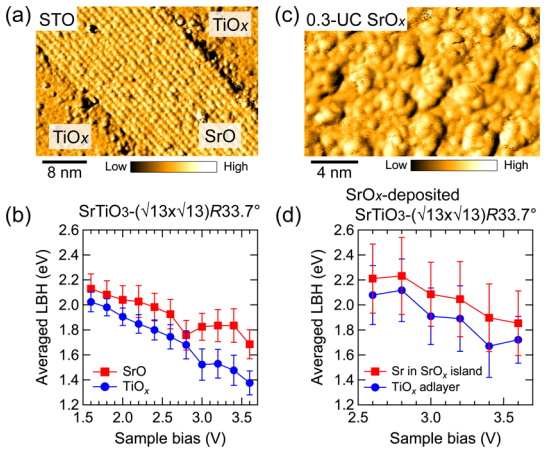

Figure 4. (a) LBH image of the STO substrate exhibiting both TiO_x adlayer and SrO [$c(6 \times 2)$] surfaces ($V_s = +3.6$ V, $I_t =$ 30 pA, 40 × 27 nm^2) . (b) LBH image of 0.3-UC SrO_x islands ($V_s = +2.6$ V, $I_t = 30$ pA, 20 × 14 nm^2). (c) LBHs of TiO_x [$(\sqrt{13} \times \sqrt{13})$ structure] and SrO [$c(6 \times 2)$] layers as a function of V_s obtained on the surface shown in (b). (d) LBHs of the SrO_x islands and the surrounding substrate surface as a function of V_s obtained on the surface shown in (c).

marginally increased with increasing V_s. For the 0.3-UC SrO_x film in Figure 4c, the LBH of the SrO_x islands was slightly higher than that of the surrounding TiO_x surface of the substrate. Furthermore, the LBH difference between them was found to be smaller than that in the STO substrate over V_s regimes studied here, which can be attributed to the intermixed chemical composition in the SrO_x islands. As mentioned above, we observed higher LBHs at SrO-terminated surface (and SrO_x islands) than those at TiO_2-terminated surface (and TiO_x substrate layer), and the difference of LBHs between SrO and TiO_2 layers becomes larger with increasing V_s as clearly seen in Figure 4b. This can explain characteristic V_s dependence of STM images (Figure 3), where SrO layer and Sr area in SrO_x islands become indistinguishable between surrounding TiO_2 layers at high V_s. This is because the larger decay rate at SrO-terminated surface and Sr in SrO_x islands would force a STM tip to approach the surface closer in order to keep a constant tunneling current, and result in, at high V_s, almost the same height or even lower height compared to surrounding TiO_x layers.

On the basis of these results, we conclude that the area showing protrusion in the STM image at $V_s = +3.5$ V is attributed to the excess Ti atoms, while the strongly suppressed area associates with SrO. Such nonuniform and noncrystalline structures were also observed in the 0.8-UC SrO_x film, confirming its inherent growth mode. This growth behavior is a striking contrast with that of STO homoepitaxy on RT13-STO substrate, in which layered structure of STO and TiO_x adlayer with RT13 structure was apparently evident.[8]

In this study, we revealed rich growth chemistry involving structural and electronic modifications in the fractional atomic-layer growth of SrO_x islands on the RT13-STO(001) surface. We stress that the microscopic pictures suggested here are applicable to general growth process on the commonly used standard STO(001) substrates, because the conventional STO substrate surface is also fully or partly reconstructed when heated at high temperature for thin films depositions, and excess Ti atoms reside on the surface,[21,22] which is, indeed, a similar situation as in the RT13-STO(001) structure. Our central finding that those excess Ti atoms are incorporated or located on the deposited layer strongly suggests the influences to the properties of ultrathin films, such as, metal-to-insulator transitions observed in 'dead layer' of a variety of perovskite oxide ultrathin films, *e.g.* $(La,Sr)MnO_3$,[23,24] $(La,Ca)MnO_3$,[25] $LaNiO_3$,[26,27] and $SrRuO_3$.[28,29] Furthermore, our results provide an important clue toward elucidating the origin of the interface-dependent transport properties of the LAO/STO interface, suggesting the inherently disordered and intermixed with excess Ti atoms, which might result in an intermixed interface[30] or alter the band and charge states at the interface when LAO layer is grown. We suggest such atomic-scale structures at the interfaces would play decisive roles in their transport properties. Control of excess species on a surface of oxide substrate or the preparation of a truly-TiO_2-terminated STO surface is of great challenges for the further development of oxide electronics.

CONCLUSIONS

We investigated atomic-scale surface and electronic structures of sub-UC SrO_x on reconstructed STO surfaces using STM. The SrO_x islands showed disordered structures as a result of the incorporation of Ti atoms. Moreover, surrounding TiO_x surfaces showed symmetry change from $(\sqrt{13} \times \sqrt{13})$ to $c(\sqrt{13} \times \sqrt{13})$, indicative of the formation of periodic defects at the surface. These growth modes were apparently different form that of the homoepitaxy on STO(001)-$(\sqrt{13} \times \sqrt{13})$-*R*33.7°. We point out that the excess atoms on oxide substrate surface should be taken into account for the comprehensive understandings of various phenomena observed in complex perovskite oxide ultrathin films and heterointerfaces. Such studies would lead to the creation of exotic electronic phenomena and functionalities utilizing the coupling between charge, spin, orbital, and lattice degrees of freedom of electrons.

EXPERIMENTAL SECTION

Niobium-doped (0.1 at%) STO(001) single crystals (Shinkosha Corp.) were used as substrates to ensure conductivity in low-temperature STM measurements. The STO substrates were prepared by using a buffered HF etch followed by annealing under an oxygen partial pressure of 1×10^{-5} Torr to produce

STO(001)-($\sqrt{13} \times \sqrt{13}$)-*R*33.7° reconstructed surfaces with step-and-terrace structures.[8,9,11] The STO-($\sqrt{13} \times \sqrt{13}$)-*R*33.7° surface structures were confirmed by reflection high-energy electron diffraction prior to film growth (Figure S1a). The SrO films were grown using PLD in a layer-by-layer manner under an oxygen partial pressure of 1×10^{-5} Torr at temperatures of 500 °C, following the report from Nishimura *et al.*[14] The growth temperatures were controlled by direct current resistive heating through the samples. Polycrystalline SrO_2 target were ablated by a KrF excimer laser (λ = 248 nm) at repetition rates of 1 Hz with laser fluence at the SrO_2 target surface set at 0.92 J/cm^2. See Supporting Information about the detailed characterization of these films. After growth, these samples were cooled to room temperature at a rate of 3−5 °C/s, followed by immediate transfer to the STM chamber without exposing the sample surfaces to air. All STM/STS measurements were conducted at 4.2 K under ultrahigh vacuum conditions, and all STM images were obtained in a constant current mode. The coverages of SrO_x films were estimated in the wide-scale STM images. The 128 × 128 and 256 × 256 points data were obtained for STS and LBH analysis, respectively. For LBH measurement, the distance (*z*) between the sample and probe tip was modulated at a frequency of 197.3 Hz and with an amplitude of 0.03 nm peak to peak. The modulated component of the tunneling current was measured by a lock-in amplifier and converted to LBH using the formula $\Phi = 0.95 \times (\mathrm{d}\ \ln I/\mathrm{d}z)^2$, where Φ and *z* are given in units of electronvolts (eV) and nanometers (nm), respectively.[20] Prior to the LBH measurements, we confirmed that the tunneling current decayed exponentially along the *z* direction, thereby ensuring an ideal vacuum gap.

Conflict of Interest: The authors declare no competing financial interest.

Acknowledgment. This study was supported by the World Premier Research Institute Initiative, promoted by the Ministry of Education, Culture, Sports, Science, and Technology of Japan (MEXT) for the Advanced Institute for Materials Research, Tohoku University, Japan. This work was also financially supported by a Grant-in-Aid for Young Scientists (A) (Grant No. 23686002) and Young Scientists (B) (Grant No. 22760021), MEXT, Japan. T.O. acknowledges financial support from the Murata Foundation. R.S. acknowledges a financial support from the Japanese Society for Promotion of Science (JSPS). We thank Patrick Han for the critical comments.

Supporting Information Available: Additional information regarding *in situ* RHEED characterization and atomic force microscope images of SrO_x thin films. This material is available free of charge *via* the Internet at http://pubs.acs.org.

REFERENCES AND NOTES

1. Ohtomo, A.; Hwang, H. Y. A High-Mobility Electron Gas at the $LaAlO_3/SrTiO_3$ Heterointerface. *Nature* **2004**, *427*, 423–426.
2. Huijben, M.; Brinkman, A.; Koster, G.; Rijnders, G.; Hilgenkamp, H.; Blank, D. H. A. Structure-Property Relation of $SrTiO_3$/$LaAlO_3$ Interface. *Adv. Mater.* **2009**, *21*, 1665–1677.
3. Thiel, S.; Hammerl, G.; Schmehl, A.; Schneider, C. W.; Mannhart, J. Tunable Quasi-Two-Dimensional Electron Gases in Oxide Heterostructure. *Science* **2006**, *313*, 1942–1945.
4. Iwaya, K.; Shimizu, R.; Hashizume, T.; Hitosugi, T. Systematic Analyses of Vibration Noise of a Vibration Isolation System for High-resolution Scanning Tunneling Microscopes. *Rev. Sci. Instrum.* **2011**, *82*, 083702.
5. Kawasaki, M.; Takahashi, K.; Maeda, T.; Tsuchiya, R.; Shinohara, M.; Ishiyama, O.; Yonezawa, T.; Yoshimoto, M.; Koinuma, H. Atomic Control of the $SrTiO_3$ Crystal Surfaces. *Science* **1994**, *266*, 1540–1542.
6. Ohsawa, T.; Iwaya, K.; Shimizu, R.; Hashizume, T.; Hitosugi, T. Thickness-Dependent Local Surface Electronic Structures of Homoepitaxial $SrTiO_3$ Thin Films. *J. Appl. Phys.* **2010**, *108*, 073710.
7. Naito, M.; Sato, H. Reflection High-Energy Electron Diffraction Study on the $SrTiO_3$ Surface Structure. *Physica C* **1994**, *229*, 1–11.
8. Shimizu, R.; Iwaya, K.; Ohsawa, T.; Shiraki, S.; Hasegawa, T.; Hashizume, T.; Hitosugi, T. Atomic-Scale Visualization of Initial Growth of Homoepitaxial $SrTiO_3$ Thin Film on an Atomically Ordered Substrate. *ACS Nano* **2011**, *5*, 7967–7971.
9. Shimizu, R.; Iwaya, K.; Ohsawa, T.; Shiraki, S.; Hasegawa, T.; Hashizume, T.; Hitosugi, T. Effect of Oxygen Deficiencies on $SrTiO_3$(001) Surface Reconstructions. *Appl. Phys. Lett.* **2012**, *100*, 263106.
10. Kienzle, D. M.; Becerra-Toledo, A. E.; Marks, L. D. Vacant-Site Octahedral Tilings on $SrTiO_3$(001), the ($\sqrt{13}\times\sqrt{13}$)*R*33.7° Surface, and Related Structures. *Phys. Rev. Lett.* **2011**, *106*, 176102.
11. Hamada, I.; Shimizu, R.; Ohsawa, T.; Iwaya, K.; Hashizume, T.; Tsukada, M.; Akagi, K.; Hitosugi, T. Imaging The Evolution of *d* States at A Strontium Titanate Surface. Submitted for publication, **2014**.
12. Jiang, Q.; Zegenhagen, J. $SrTiO_3$(001)-*c*(6 × 2): A Long-Range, Atomically Ordered Surface Stable in Oxygen and Ambient Air. *Surf. Sci.* **1996**, *367*, L42–L46.
13. Iwaya, K.; Shimizu, R.; Ohsawa, T.; Hashizume, T.; Hitosugi, T. Stripe Charge Ordering in SrO-terminated $SrTiO_3$(001) Surfaces. *Phys. Rev. B* **2011**, *83*, 125117.
14. Nishimura, J.; Ohtomo, A.; Ohkubo, A.; Murakami, Y.; Kawasaki, M. Controlled Carrier Generation at a Polarity-Discontinued Perovskite Heterointerfaces. *Jpn. J. Appl. Phys.* **2004**, *43*, L1032–L1034.
15. Reed, T. B. Free Energy of Formation of Binary Compounds. In *An Atlas of Charts for High-Temperature Chemical Calculations*; MIT Press: Cambridge, MA, 1971.
16. Wendt, S.; Schaub, R.; Matthiesen, J.; Vestergaard, E. K.; Wahlström, E.; Rasmussen, M. D.; Thostrup, P.; Molina, L. M.; Lægsgaard, E.; Stensgaard, I.; *et al.* Oxygen Vacancies on TiO_2(110) and Their Interaction with H_2O and O_2: A Combined High-Resolution STM and DFT Study. *Surf. Sci.* **2005**, *598*, 226–245.
17. Ohsawa, T. *et al.* Manuscript in preparation.
18. Kurokawa, S.; Yuasa, M.; Sakai, A.; Hasegawa, Y. Barrier-Height Imaging of Oxygen-Adsorbed Si(111) 7 × 7 Surface. *Jpn. J. Appl. Phys* **1997**, *36*, 3860–3863.
19. Cygan, M. T.; Dunbar, T. D.; Arnold, J. J.; Bumm, L. A.; Shedlock, N. F.; Burgin, T. P.; Jones, L., II; Allara, D. L.; Tour, J. M.; Weiss, P. S. Insertion, Conductivity, and Structures of Conjugated Organic Oligomers in Self-Assembled Alkanethiol Monolayers on Au(111). *J. Am. Chem, Soc* **1998**, *120*, 2721–2732.
20. Wiesendanger, R. *Scanning Probe Microscopy and Spectroscopy*; Cambridge University Press: Cambridge, U.K., 1994.
21. Erdman, N.; Poeppelmeier, K. R.; Asta, M.; Warschkow, O.; Ellis, D. E.; Marks, L. D. The Structure and Chemistry of the TiO_2-Rich Surface of $SrTiO_3$(001). *Nature* **2002**, *419*, 55–58.
22. Zhu, G.-Z; Radtke, G.; Botton, G. A. Bonding and Structure of a Reconstructed (001) Surface of $SrTiO_3$ from TEM. *Nature* **2012**, *490*, 384–387.
23. Sun, J. Z.; Abraham, D. W.; Rao, R. A.; Eom, C. B. Thickness-Dependent Magnetotrasnport in Ultrathin Manganite Films. *Appl. Phys. Lett.* **1999**, *74*, 3017.
24. Hong, X.; Posadas, A.; Ahn, C. H. Examining the Screening Limit of Field Effect Devices *via* the Metal-Insulator Transition. *Appl. Phys. Lett.* **2005**, *86*, 142501.
25. Shimizu, R.; Ohsawa, T.; Iwaya, K.; Shiraki, S.; Hitosugi, T. Epitaxial growth process of $La_{0.7}Ca_{0.3}MnO_3$ Thin Films on $SrTiO_3$ (001): Thickness-Dependent Inhomogeneity Caused by Excess Ti Atoms. *Cryst. Growth Des.* **2014**, 10.1021/cg4013119.
26. Scherwitzl, R.; Zubko, P.; Lichtensteiger, C.; Triscone, J.-M. Electric-Field Tuning of the Metal-Insulator Transition in Ultrahin Films of $LaNiO_3$. *Appl. Phys. Lett.* **2009**, *95*, 222114.
27. Son, J.-W.; Moetakef, P.; LeBeau, J. M.; Ouellette, D.; Balents, L.; Allen, S. J.; Stemmer, S. Low-Dimensional Mott Material: Transport in Ultrathin Epitaxial $LaNiO_3$ Films. *Appl. Phys. Lett.* **2010**, *96*, 062114.
28. Toyota, D.; Ohkubo, I.; Kumigashira, H.; Oshima, M.; Ohnishi, T.; Lippmaa, M.; Takizawa, M.; Fujimori, A.; Ono,

K.; Kawasaki, M.; Koinuma, H. Thickness-Dependent Electronic Structure of Ultrathin $SrRuO_3$ Films Studied by *in Situ* Photoemission Spectroscopy. *Appl. Phys. Lett.* **2005**, *87*, 162508.
29. Xia, J.; Siemons, W.; Koster, G.; Beasley, M. R.; Kapitulnik, A. Critical Thickness for Itinerant Ferromagnetism in Ultrathin Films of $SrRuO_3$. *Phys. Rev. B* **2009**, *79*, 140407(R).
30. Chambers, S. A.; *et al.* Instability, Intermixing and Electronic Structure at the Epitaxial $LaAlO_3/SrTiO_3$(001) Heterojunction. *Surf. Sci. Rep.* **2010**, *65*, 317–352.